JCTC Journal of Chemical Theory and Computation

Article

pubs.acs.org/JCTC

The Self-Association of Graphane Is Driven by London Dispersion and Enhanced Orbital Interactions

Changwei Wang,[#] Yirong Mo,*[,‡] J. Philipp Wagner,[§] Peter R. Schreiner,*[,§] Eluvathingal D. Jemmis,*[,∥] David Danovich,[⊥] and Sason Shaik*[,⊥]

[#]Department of Chemistry, School of Science, China University of Petroleum (East China), Changjianxi Road 66, 266580 Tsingtao, China

[‡]Department of Chemistry, Western Michigan University, Kalamazoo, Michigan 49008, United States

[§]Institute of Organic Chemistry, Justus-Liebig University, Heinrich-Buff-Ring 58, 35392 Giessen, Germany

[∥]Department of Inorganic and Physical Chemistry, Indian Institute of Science, Bangalore 560012 India

[⊥]Institute of Chemistry and Lise Meitner Minerva Center for Computational Quantum Chemistry, The Hebrew University, Jerusalem 91904, Israel

Supporting Information

ABSTRACT: We investigated the nature of the cohesive energy between graphane sheets via multiple CH···HC interactions, using density functional theory (DFT) including dispersion correction (Grimme's D3 approach) computations of [*n*]graphane σ dimers (n = 6−73). For comparison, we also evaluated the binding between graphene sheets that display prototypical π/π interactions. The results were analyzed using the block-localized wave function (BLW) method, which is a variant of *ab initio* valence bond (VB) theory. BLW interprets the intermolecular interactions in terms of frozen interaction energy (ΔE_F) composed of electrostatic and Pauli repulsion interactions, polarization (ΔE_{pol}), charge-transfer interaction (ΔE_{CT}), and dispersion effects (ΔE_{disp}). The BLW analysis reveals that the cohesive energy between graphane sheets is dominated by two stabilizing effects, namely intermolecular London dispersion and two-way charge transfer energy due to the $\sigma_{CH} \rightarrow \sigma^*_{HC}$ interactions. The shift of the electron density around the nonpolar covalent C−H bonds involved in the intermolecular interaction decreases the C−H bond lengths uniformly by 0.001 Å. The ΔE_{CT} term, which accounts for ∼15% of the total binding energy, results in the accumulation of electron density in the interface area between two layers. This accumulated electron density thus acts as an electronic "glue" for the graphane layers and constitutes an important driving force in the self-association and stability of graphane under ambient conditions. Similarly, the "double faced adhesive tape" style of charge transfer interactions was also observed among graphene sheets in which it accounts for ∼18% of the total binding energy. The binding energy between graphane sheets is *additive* and can be expressed as a sum of CH···HC interactions, or as a function of the number of C−H bonds.

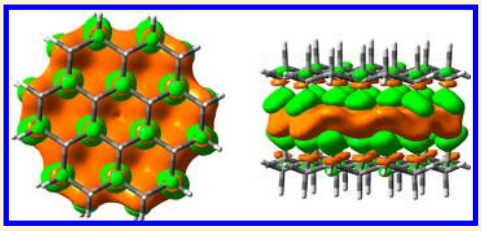

INTRODUCTION

The addition of hydrogen to highly conductive graphene produces saturated graphane corrugated sheets possessing C−H bonds,[1−5] which are perpendicular to the two carbon-planes of the sheet. Ever since its first experimental realization in 2009,[3] graphane has attracted increasing attention as a novel material with great potential in the field of two-dimensional nanocarbons.[6,7] For instance, some of its applications are explored in transistor design,[8,9] biosensing,[10] and hydrogen storage.[11,12]

In the meantime, extensive theoretical studies of pure or doped graphanes have been performed to reveal their mechanical, thermal, electronic, optical, and magnetic properties.[13−22] It is generally expected that the binding among graphane layers as well as the crystallization of graphane, for which there are no experimental but only theoretical reports so far,[23] is driven by dispersive CH···HC interactions, i.e., the attractive portion (or London dispersion) of the van der Waals (vdW) interaction. Despite the weakness of these noncovalent π/π (graphenes) and σ/σ (graphanes) interactions,[24] their accumulation may well result in strong overall bonding, as found in protein interactions, host−guest interactions, hydrocarbons in condensed states, and self-assembly. Understanding these weak forces can play a guiding role in the design of new, stable self-assembling materials and in the refinement of force fields.[25−28]

Using the attractive dispersion interactions between diamondoid dimers, one of us (P.R.S.) synthesized compounds with the longest alkane C−C bond (up to 1.71 Å),[29,30] reported to date, and showed that the extraordinary stability of these compounds (with melting points far above 200 °C) originates from highly favorable CH···HC interactions. This experimental observation was rationalized by DFT computations with and

Received: January 27, 2015

DOI: 10.1021/acs.jctc.5b00075
J. Chem. Theory Comput. XXXX, XXX, XXX−XXX

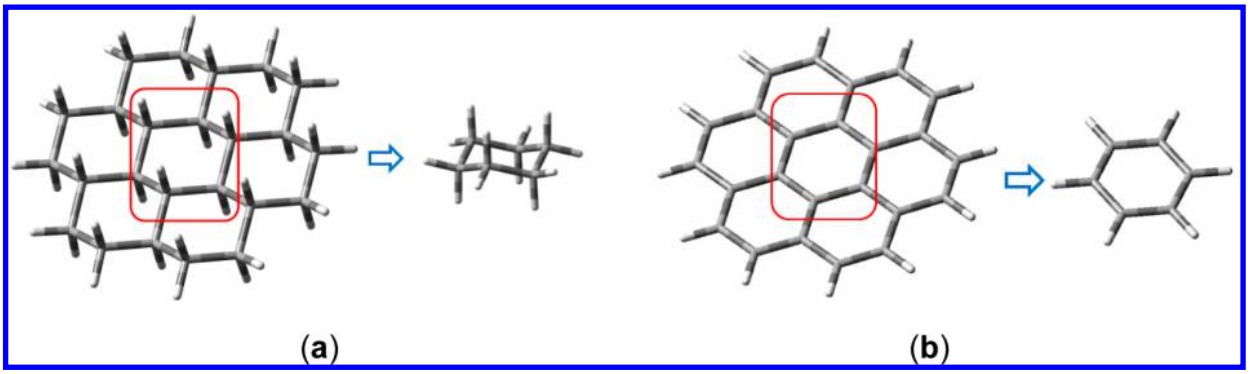

Figure 1. [24]graphane monomer and the unit cell C_6H_{12} (a) vs [24]graphene and the unit cell C_6H_6 (b).

without dispersion corrections.[29,30] It was further shown mostly by DFT computations[24] that the CH···HC interactions in multilayered [*n*]graphanes are as important as the π/π interactions in the unsaturated analogues. This important finding was confirmed by a high level CCSD(T) benchmark study,[31] though the binding energies of graphanes are lower than those of the graphenes with increasing system size: [24]graphane reaches only 67% of the binding energy of [24]graphene. In accord with that, Grimme showed that special electron correlation effects exist between π systems with more than 10 carbon atoms and consequently enable these systems to exhibit extraordinary London dispersion interactions.[32] Two of us (D.D. and S.S.)[33] used ab initio valence bond (VB) theory to study the nature of the CH···HC interactions in alkane dimers. This study demonstrated that an essential part of the cohesive energy results from the charge transfer and recoupling of the electrons of the original CH bonds.[33] Recently, this was verified by energy decomposition analysis (EDA) of small graphane model systems showing that the CH···HC interactions involve, in addition to dispersion, also orbital interaction components.[34] All of these results call for a general study of the nature of the sheet−sheet interactions in a large [*n*]graphane series, with an attempt to understand the nature of the CH···HC interactions and their behavior when *n* is extrapolated to infinity. The nature of the CH···HC interactions will be compared to the corresponding C(π)···C(π) interactions in graphenes. This is done here by using the block-localized wave function (BLW) method,[35−37] which quantifies the energy contributions to the cohesive energies of [*n*]-graphane sheets in which *n* runs from 6 all the way to 73.

As the simplest variant of ab initio valence bond (VB) theory, the BLW method defines the intermediate electron-localized state self-consistently, which can thus be used as a reference state for exploring the nature of intermolecular interactions in terms of several physically intuitive energy components.[35−37] The resulting BLW-EDA method is similar to the Morokuma−Kitaura energy decomposition scheme[38,39] and other EDA methods.[40−52] As already demonstrated, both the polarization and charge transfer energies are affected little by the inclusion of dispersion.[53] Thus, dispersion can be regarded as an independent energy component in EDA, and it can be used as an add-on to the BLW-EDA analysis of dispersion corrected density functional theory (DFT) computations of various types (see Computational Strategy and Methods section). While our analyses concur with the view that dispersion is the primary cause of the graphane−graphane and graphene−graphene cohesions, *the results also reveal that charge-transfer binding plays a secondary yet important role* as deduced before in explicit VB computations[33] and in an EDA analysis[34] of small model systems. Specifically, the two-way and symmetric electron transfer between the interacting CH bonds results in *the accumulation of electron density in the common area, i.e., the boundary area between two layers, which acts like an electronic "glue" for the graphane layers* and helps in the self-association of graphane. Similar two-way charge transfer binding was identified in graphene−graphene bindings as well.

COMPUTATIONAL STRATEGY AND METHODS

Investigated Systems. For consistency, we only considered graphanes in their most favorable chairlike connectivity and edge conformation.[1,2] In Figure 1, [24]graphane and its unit cell (supplemented with six hydrogen atoms to form cyclohexane C_6H_{12}) as well as [24]graphene (i.e., coronene) and its unit cell (supplemented with six hydrogen atoms to form benzene C_6H_6) are depicted as illustrative examples. We constructed dimers of [6]-, [10]-, [13]-, [16]-, [24]-, [27]-, [33]-, [37]-, [46]-, [54]-, [57]-, [61]-, and [73]graphanes and for comparison also parallel displaced dimers of [6]-, [10]-, [14]-, [16]-, [24]-, [32]-, and [42]graphenes.

All envisioned dimer and monomer geometries were optimized at the B3LYP/6-31G(d,p) level of theory augmented by Grimme's D3-dispersion correction but without BSSE corrections.[54−56]

One has to recognize here that it is an intricate theoretical challenge to model σ/σ and π/π interactions equally well, especially for the system sizes that are investigated in this study.[32] Grimme's D3 dispersion correction provides an elegant solution to this problem as it takes into account the hybridization states of the interacting atoms. For instance, Janowski and Pulay could reproduce their CCSD(T) benchmark geometries and binding energies of even [24]graphane and [24]graphene dimers very well with the B3LYP-D3/aug-cc-pVDZ method.[31] Thus, we also decided to choose B3LYP-D3 together with a double-ζ basis set. However, we avoided the use of diffuse functions for the sake of computational manageability. All DFT geometry optimizations were performed with GAMESS,[57] and the subsequent BLW geometry optimizations and energy decomposition analyses were performed with the in-house version of GAMESS[57] to which the BLW method was ported.

Methods and Procedures. Test computations of the benzene dimer and the cyclohexane dimer indicate that B3LYP-D3/6-31G(d,p) computations lead to intermolecular distances comparable to those of high-level theory. As can be seen from Figure 2, the DFT method reproduces the distances R_1 and R_2 obtained from coupled cluster computations well; these values

DOI: 10.1021/acs.jctc.5b00075
J. Chem. Theory Comput. XXXX, XXX, XXX−XXX

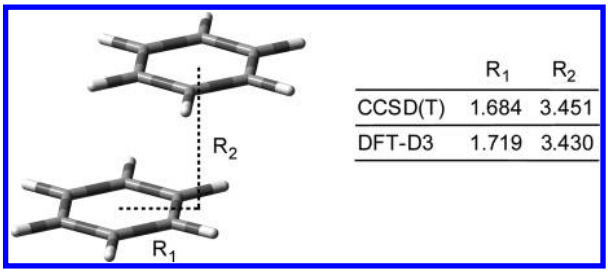

	R_1	R_2
CCSD(T)	1.684	3.451
DFT-D3	1.719	3.430

Figure 2. Key structural parameters (Å) at the CCSD(T)/aug-cc-pVTZ and B3LYP(VWN5)-D3/6-31G(d,p) levels for the parallel displaced benzene dimer.

define shift and distance of benzene monomers in the parallel-displaced dimer. The same is true for the cyclohexane dimer: the intermolecular H···H distance at the CCSD(T) level is 2.42 Å,[58] while our computations led to an acceptable value of 2.37 Å. Energetically, however, the employed DFT method on one hand overestimates the binding energies compared with CCSD(T) results for graphane dimers and, on the other hand, underestimates the binding energies in graphene dimers. Analyses of the benzene dimer show that the primary culprit is the large basis set superposition error (BSSE) encountered for the B3LYP method, as the energy of the electron localized diabatic state (BLW) is even lower than the energy of the electron delocalized adiabatic state whose BSSE is corrected by the standard counterpoise method.[59] This physically incorrect result suggests that the counterpoise method exaggerates the BSSE for graphene dimers. As such, we decided to scale the BSSE to make the final B3LYP binding energies in these two test dimers the same as the CCSD(T)/CBS values (−11.3 kJ mol^{-1} for the cyclohexane dimer and −11.3 kJ mol^{-1} for the benzene dimer) obtained by Granatier et al.[28] The resulting BSSE scaling factors 1.3806 and 0.4922 for the B3LYP-(VWN5)-D3/6-31G(d,p) computations were used for all graphane and graphene dimers, respectively, throughout the work.

The BLW Method. In the BLW-EDA method, the binding energy ΔE_b between two monomers A and B is defined as the sum of deformation energy ΔE_{def} and the intermolecular interaction energy ΔE_{int}:

$$\Delta E_b = \Delta E_{def} + \Delta E_{int} \quad (1)$$

The deformation energy refers to the energetic cost for deforming the monomers from their separated minimum energy structures to their distorted geometries in the optimized structure of the AB dimer.

The interaction energy ΔE_{int} is the energy difference between the dimer and the sum of the individual energies of monomers with the correction of the BSSE, which is evaluated by the scaled counterpoise method.[59] The total interaction energy can be further decomposed into its components as shown in eq 2:

$$\begin{aligned}\Delta E_{int} &= E(\Psi_{AB}) - E(\Psi_A^0) - E(\Psi_B^0) + \text{BSSE} \\ &= \Delta E_F + \Delta E_{pol} + \Delta E_{CT} + \Delta E_{disp}\end{aligned} \quad (2)$$

Here, ΔE_F is the frozen energy contribution, defined as the energy change by bringing monomers together without disturbing (i.e., freezing) their individual geometries and electron densities; in the present cases, the term is positive and thus largely reflects the repulsive Pauli exchange contribution. The polarization energy ΔE_{pol} corresponds to the energy contribution as a result of the electron density redistribution within each monomer due to the electric field imposed by the other monomer. The extension of electron reorganization from individual monomers to the whole complex further stabilizes the dimers, and the accompanied energy change, after the BSSE correction, is denoted as the charge transfer energy ΔE_{CT}, albeit it includes other effects due to electronic reorganization in the interacting, e.g., CH···HC bonds.[33] Finally, the dispersion contribution to dimerization is computed with Grimme's dispersion correction[54−56] by reference to the sum of the dispersion energies of the monomers within the dimer geometry. For the sake of lucidity, the sum of ΔE_{def}, ΔE_F, ΔE_{pol}, and ΔE_{disp} is grouped together as the steric energy (ΔE_s). Thus, overall, the binding energy can be expressed as a sum of a "steric" contribution and quantum chemical contribution due to electronic charge transfer interaction:

$$\Delta E_b = \Delta E_s + \Delta E_{CT} \quad (3)$$

The derivation of these individual energy terms is based on the construction of the initial block-localized wave function for the dimer ψ_{AB}^{BLW0} as well as its self-consistent form ψ_{AB}^{BLW} as

$$\Psi_{AB}^{BLW0} = \hat{A}(\Psi_A^0 \Psi_B^0) \quad (4a)$$

$$\Psi_{AB}^{BLW} = \hat{A}(\Psi_A \Psi_B) \quad (4b)$$

RESULTS AND DISCUSSION

Geometries of Dimers. We first examined the distances between two graphane layers as defined in Figure 3, where *d*

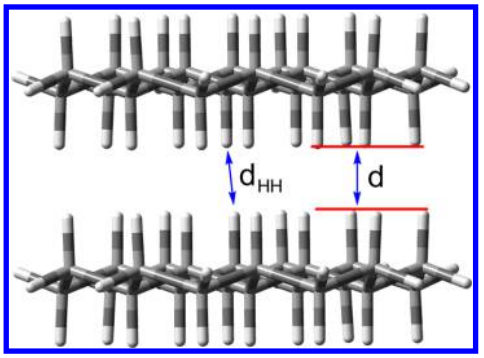

Figure 3. Definition of the distance between two graphane layers.

measures the distances between two parallel nearest planes of hydrogen atoms and d_{HH} is the distance between two nearest hydrogen atoms. While the regular DFT optimization considers both steric and charge transfer effects, the optimization of the reference BLW state reflects the purely steric factors (eq 4), i.e., the van der Waals effect, whereas the electron transfer between the layers is completely quenched. The difference between the distances derived from DFT and BLW optimizations thus provides a glimpse of the weight of the electron transfer interaction in the vdW graphane dimers. Table 1 compares the distances and binding energies for the dimers of methane and [*n*]graphanes (*n* = 6, 10, 13, 16, and 24). For the [24]graphane dimer, the binding energy at a high level of theory is reproduced quite well (64.8 kJ mol^{-1} vs 56.9 kJ mol^{-1} in Janowski and Pulay's study[31]), while the distance d_{HH} is somewhat underestimated (2.33 Å vs 2.50 Å).

Table 1 shows that with the enlargement of [*n*]graphanes the distance between two layers gradually converges to a finite

DOI: 10.1021/acs.jctc.5b00075
J. Chem. Theory Comput. XXXX, XXX, XXX−XXX

Table 1. H···H Distances (Å) and Binding Energies (kJ mol^{-1}) in [n]graphane Dimers (n = 6, 10, 13, 16, and 24) from Regular DFT and BLW Optimizations, Both at the B3LYP(VWN5)-D3/6-31G(d,p) Level

	d(DFT)	d_{HH}(DFT)	d(BLW)	d_{HH}(BLW)	ΔE_b	ΔE_b(BLW)	$\Delta\Delta E_b$[a]
$H_3CH\cdots HCH_3$	2.425	2.425	2.607	2.607	−0.9	−0.7	0.2
[6]dimer	1.799	2.375	1.872	2.427	−11.4	−10.0	1.4
[10]dimer	1.706	2.367	1.777	2.423	−21.8	−19.0	2.8
[13]dimer	1.828	2.343	1.903	2.427	−30.6	−26.9	3.7
[16]dimer	1.847	2.354	1.918	2.418	−39.5	−34.5	5.0
[24]dimer	1.830	2.333	1.928	2.410	−64.7	−56.8	7.9

[a] $\Delta\Delta E_b = \Delta E_b(\text{BLW}) - \Delta E_b$.

Table 2. Computed Contributions of Energy Components to the Binding Energy in the Optimized Geometries of Graphane Dimers at the B3LYP(VWN5)-D3/6-31G(d,p) Level with the BLW-EDA Approach (kJ mol^{-1})

N	ΔE_{def}	ΔE_F	ΔE_{disp}	ΔE_{pol}	ΔE_s	ΔE_{CT}	ΔE_{int}	ΔE_b
6	0.0	12.0	−21.5	−0.2	−9.7	−1.9	−11.6	−11.6
10	0.1	22.0	−39.9	−0.4	−18.2	−3.6	−21.9	−21.8
13	0.0	29.4	−54.5	−0.5	−25.6	−4.9	−30.5	−30.5
16	0.0	37.1	−69.6	−0.7	−33.2	−6.3	−39.5	−39.5
24	0.0	58.7	−112.2	−1.3	−54.8	−10.0	−64.8	−64.8
27	0.3	66.9	−125.2	−1.4	−59.4	−11.3	−71.0	−70.7
33	0.2	82.5	−159.1	−1.8	−78.2	−14.2	−92.6	−92.4
37	0.4	93.5	−177.0	−2.1	−85.2	−15.8	−101.4	−101.0
46	0.6	118.2	−230.2	−2.7	−114.1	−20.4	−135.1	−134.5
54	0.5	142.6	−279.7	−3.4	−140.0	−24.6	−165.1	−164.6
57	0.5	140.3	−275.2	−2.8	−137.2	−24.2	−161.9	−161.4
61	0.7	160.0	−313.9	−3.8	−157.0	−27.8	−185.5	−184.8
73	0.7	187.4	−368.0	−3.9	−183.8	−32.5	−217.0	−216.3

Table 3. Computed Contributions of Energy Components to the Binding Energy in the Optimized Geometries of Graphene Dimers at the B3LYP(VWN5)-D3/6-31G(d,p) Level with the BLW-EDA Approach (kJ mol^{-1})

n	ΔE_{def}	ΔE_F	ΔE_{disp}	ΔE_{pol}	ΔE_s	ΔE_{CT}	ΔE_{int}	ΔE_b
6	0.2	15.6	−23.1	−0.7	−8.0	−3.3	−11.5	−11.3
10	0.3	27.6	−45.9	−1.0	−19.0	−6.3	−25.6	−25.3
14	0.3	36.2	−65.6	−1.3	−30.4	−6.4	−37.1	−36.8
16	0.4	44.2	−81.4	−1.4	−38.2	−9.6	−48.2	−47.8
24	0.5	67.7	−133.1	−1.7	−66.6	−15.9	−83.0	−82.5
32	0.7	93.4	−187.4	−2.0	−95.3	−23.1	−119.1	−118.4
42	1.0	121.3	−253.5	−2.3	−133.5	−30.1	−164.6	−163.6

value (though computations of even larger dimers are needed here, but the BLW optimizations with van der Waals terms in, but without charge transfer along very flat energy profiles, are difficult to converge). The regular DFT optimizations for the two parallel planes of hydrogen atoms converge to 1.83 Å while the BLW optimizations at the same theoretical level converge to 1.93 Å. The difference (0.10 Å) underscores the contribution of the electron transfer effects to the tightening of the CH···HC distances. It is illuminating to compare the nearest H···H distances (d_{HH}), which converge to 2.33 and 2.41 Å during the DFT and BLW optimizations, respectively. The BLW optimal values, which are larger than DFT distances, essentially correspond to the van der Waals distances.

Energy Contributions to the Stability of Dimers. Energy decomposition analyses for the DFT optimized dimers are compiled in Tables 2 and 3; three notable findings should be pointed out:

(a) First, the frozen state energy term (ΔE_F) is positive for all systems. Since this energy term is composed of the electrostatic interaction and the Pauli repulsion with partial electron correlation, its positive values indicate a large destabilizing Pauli exchange repulsion between the layers of graphanes or graphenes.

(b) Second, the intermolecular dispersion term (ΔE_{disp}) plays a dominating and stabilizing role in the dimerization of graphanes or graphenes. The dominance of the dispersion interaction is expected for saturated graphanes, which are nonpolar and where van der Waals interactions are supposed to be the primary force for the aggregation.

(c) A third finding is the significant charge transfer energy. The contribution of the ΔE_{CT} term to the binding energy slowly decreases and converges to 15% in graphanes and 18% in graphenes.

As has been shown previously, there is a linear relationship between the total binding energy and the number of carbon atoms[24] — a fact that confirms the additive nature of σ/σ interactions.[34,60] To further shed light on this fact, we plotted in Figure 4 the energy contributions of single components of the interaction energy divided by the total binding energy ($\Delta E_i/\Delta E_b$) vs the number of carbon atoms in a graphane sheet. In all the cases in the figure, the relative contribution changes minimally with the number of carbons but converges to a finite value.

DOI: 10.1021/acs.jctc.5b00075
J. Chem. Theory Comput. XXXX, XXX, XXX−XXX

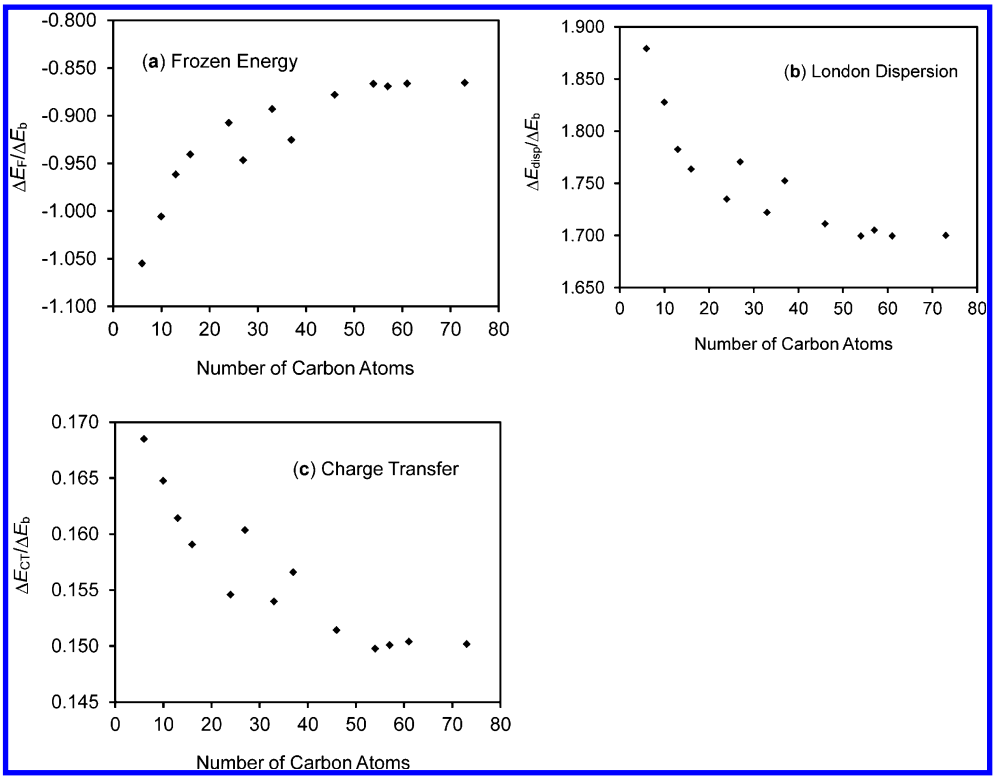

Figure 4. Trends of the ratios of various component energies to the total binding energy, $\Delta E_i/\Delta E_b$, as a function of the number of carbon atoms in a graphane sheet: (a) Frozen energy component, ΔE_F. (b) London dispersion energy component ΔE_{disp}, and (c) the charge transfer energy component, ΔE_{CT}. The two outliers (n = 27 and 37) are due to the relatively unfavorable interactions between [27] or [37]graphane sheets (see in Table 2: the bonding energies of the outliers are very close to [24] and [33]graphane dimers, respectively).

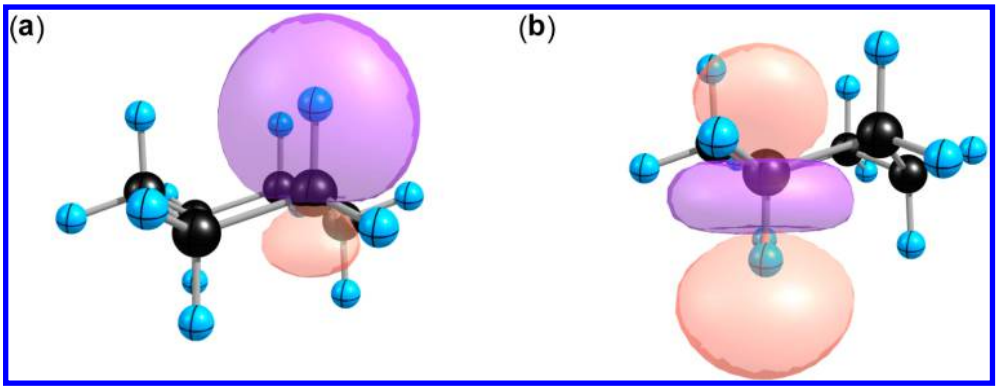

Figure 5. Natural bond orbitals at the HF/cc-pVQZ level of theory: (a) a bonding donor σ_{CH} orbital and an antibonding σ_{CH}* acceptor orbital (b).

We attribute these changes to the change in chemical nature of the C−H bonds in the graphanes: [6]graphane is made up to 100% of secondary carbons while [73]graphane mainly consists of tertiary carbons and some residual secondary carbons at the vertices (29% of all carbon atoms are secondary). However, as the sheet grows, these differences disappear and the $\Delta E_i/\Delta E_b$ values converge.

In the hyperconjugation concept,[61] one assumes some charge transfer from an occupied C−H bonding orbital to an adjacent, periplanar C−H antibond orbital, i.e., $\sigma_{CH} \rightarrow \sigma_{HC}$*, even in ethane, though there have been controversies over the magnitude of this kind of hyperconjugative interaction.[62−66] The BLW method, following Mulliken's original proposal by limiting the eight electrons of e symmetry which are involved in hyperconjugative interactions to two sets of methyl group functions (i.e., disabling any hyperconjugative orbital interactions),[67] showed the hyperconjugation energy to be about 27.6−30.5 kJ mol^{-1} in the eclipsed and staggered conformers of ethane.[68]

The respective NBO values are 65.3−94.1 kJ mol^{-1}. Unlike the shoulder-to-shoulder orientations of the C−H bonds in alkanes, the C−H bonds in the graphane dimers approach each other in a head-to-head way. To further support this charge-transfer assisted mechanism of dimer formation, we performed also a natural bond orbital analysis with NBO3.1.[69,70] The second order perturbation theory analysis of the Fock matrix in the NBO basis indeed reveals that $\sigma_{CH} \rightarrow \sigma_{HC}$* resonances are the dominant intermolecular charge transfer interactions. For cyclohexane, every axial C−H bond donates partial electrons equally into two σ_{CH}* antibonding orbitals of the axial hydrogens in the other monomer; i.e., the charge transfer is very local. The interacting natural bond orbitals are depicted in

DOI: 10.1021/acs.jctc.5b00075
J. Chem. Theory Comput. XXXX, XXX, XXX−XXX

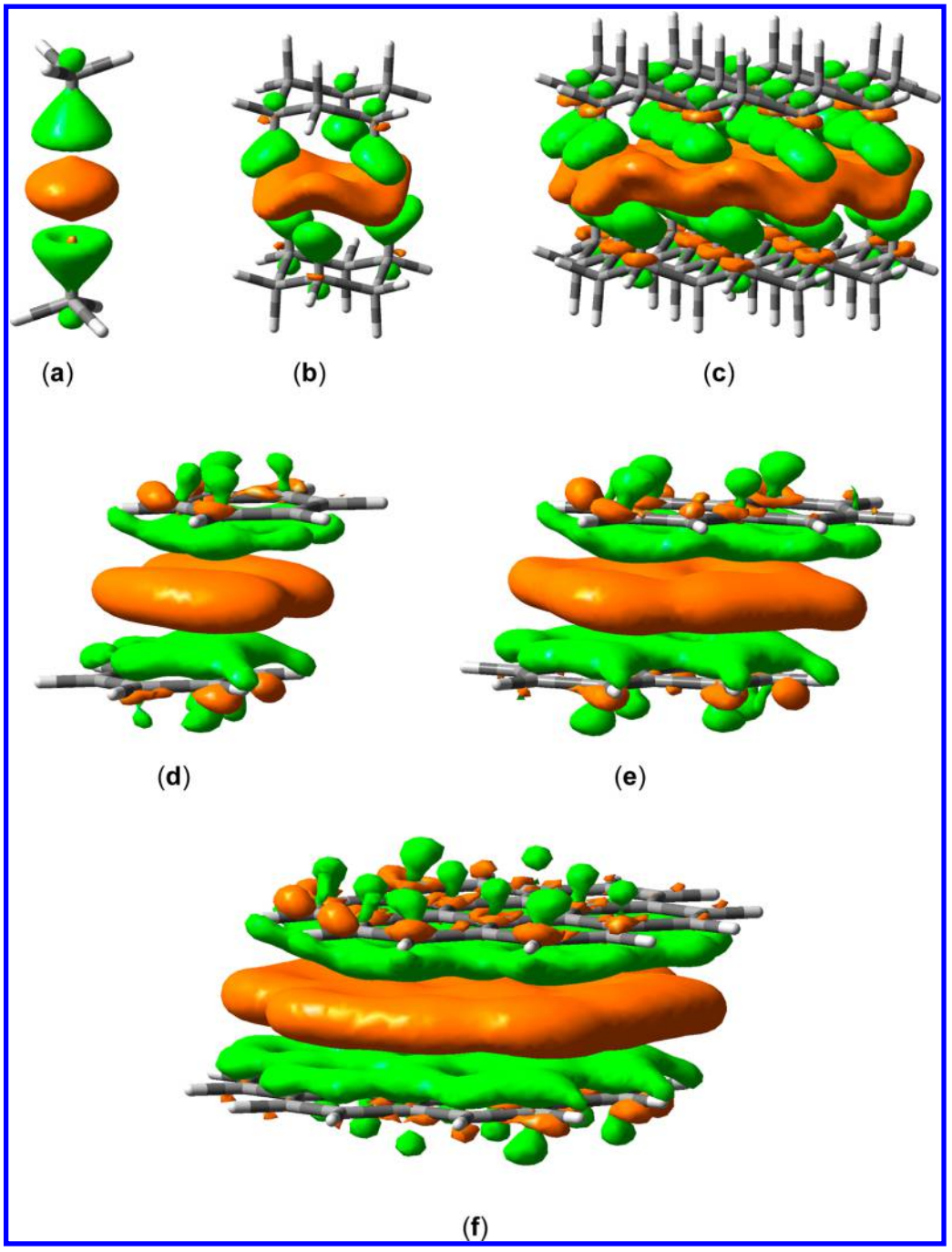

Figure 6. Electron density difference (EDD) maps for the charge-transfer effect in the dimers of (a) methane, (b) cyclohexane, (c) [24]graphane, (d) benzene, (e) [10]graphene, and (f) [24]graphene dimers, with an isodensity value of 0.0001 au. The orange color indicates an increase while the green color, a reduction of electron density.

Figure 5. One can see that the orbital coefficients of both NBOs are still large outside the plane of the axial hydrogens making sufficient intermolecular overlap possible. Of course, the transfer happens in both ways with each of the described interactions contributing 0.3 kJ mol^{-1} at the HF/cc-pVQZ level of theory on the most stable geometry from a MP2/cc-pVQZ rigid monomer distance scan (shown in the Supporting Information). Deleting all intermolecular CT interactions, the entire interaction energy between the two cyclohexane monomers is computed to be positive, +16.7 kJ mol^{-1}, meaning that *the cyclohexane dimer would be unbound without the charge transfer interaction*! Thus, despite the nice qualitative agreement of our major workhorse, the BLW method, and the NBO method, there is a substantial disagreement about the magnitude of the CT interaction, largely due to the fact that natural bond orbitals are not allowed to relax (only one SCF cycle is performed). Therefore, the NBO value defines an upper bound of the charge-transfer energy contribution to the binding. In contrast to that, the BLW method uses a self-consistent wave function and produces more reliable quantitative results.

All in all, the accumulation of the many $\sigma_{CH} \rightarrow \sigma_{HC}^*$ interactions accounts for about one-sixth of the total binding energy based on our BLW computations. In line with this

DOI: 10.1021/acs.jctc.5b00075
J. Chem. Theory Comput. XXXX, XXX, XXX−XXX

conclusion, modern ab initio VB studies of alkanes show that, apart from the oscillating dipoles as the source of dispersion interactions, there is a reorganization of bonding electrons in the two interacting C−H bonds.[33]

The VB resonance structures corresponding to the latter electron reorganization can be regarded as charge-transferred structures due to the recoupling of electrons in the two CH bonds. These charge-transferred (or electron recoupling) structures make an important contribution to the intermolecular CH···HC binding of alkanes with tertiary C−H bonds. These VB results are in accord with the present BLW studies of the graphane dimers. The reorganization of electron density in each of the C−H bonds dominated by polarization caused by the approaching C−H bond shortens the C−H bonds and blue-shifts their stretching vibrational frequencies,[71,72] and this happens only for nonpolar X−H bonds. The electron density around the H of C−H is pushed into the bonding region. In polar X−H bonds, the electron density is already polarized toward X, and the electron transfer process $\sigma_{XH} \rightarrow \sigma_{XC}^*$ dominates. The magnitude of the decrease of C−H bond lengths is small, and the average shortening of 0.001 Å observed here (see Table S6) is in tune with what was anticipated.

The electron densities of the DFT vs BLW computations correspond to the electron-delocalized vs electron-localized states, respectively. As such, the difference between these electron densities would provide the electron density flow due to the charge transfer effect. Figure 6 plots the electron density difference (EDD) maps for the dimers of methane, cyclohexane, and [24]graphane. The electron transfer interaction is very local; i.e., the changes occur only in the interacting C−H bonds, which is supported by our NBO results. Due to the two-way and symmetric $\sigma_{CH} \rightarrow \sigma_{HC}^*$ electron transfer interactions, there is a loss of electron density from interacting C−H bonds (in green). The lost density moves to the boundary area between two layers (in orange) and looks like a "double faced adhesive tape," gluing the graphane layers together. This adhesive contributes to the dimerization and stability of graphane dimers. We note that this picture is different from the one presented by Rohrer and Hyldegard, who concluded that the charge rearrangements are not accompanied by density enhancement in the middle region. This conclusion was based on their comparison of the density distributions in the dimer and the summation of monomers.[73] Clearly, the latter quantity corresponds essentially to the sum of polarization and charge transfer effects in our analyses. In other words, polarization diminishes the electron density in the middle region with the approaching of two sheets, but the two-way electron transfer interaction enhances the electron density in the middle region. Since the polarization effect is insignificant in the binding of graphane or graphene sheets (see Tables 2 and 3), what remains therefore is only the charge transfer effect as the contributor to the adhesive glue of the layers.

A Group-Additivity Scheme. A group additivity scheme was the starting point of empirical force fields for covalent organic molecules.[74] Inspired by this achievement, we may reconsider our present data with an aim of formulating an empirical value for the binding energy per C−H interaction. If the peripheral C−H bonds (the equatorial C−H bonds) are ignored, then half of the remaining C−H bonds of a given graphane sheet point to the neighboring graphane sheet. As the size of the graphane increases, the impact of the peripheral C−H bonds becomes negligible compared with the axial C−H bonds that glue the layers. Let us therefore consider only the axial C−H bonds between the graphane sheets.

As noted already, the axial C−H bonds of one sheet are not collinear with the C−H bonds of the adjacent sheet but displaced in such a way that each C−H bond sees three neighbors from the adjacent sheet. Table 4 compiles the number of C−H bonds on one side of the graphane sheet (N_{CH}), the number of CH···HC interaction involving one C−H group ($N_{CH\cdots HC}$), the binding energy (ΔE_b), the binding energy per CH bond, N_{CH} ($\Delta E_b/N_{CH}$), and binding energy per CH···HC ($\Delta E_b/N_{CH\cdots HC}$) interaction. As the value of n increases, the $\Delta E_b/N_{CH}$ and $\Delta E_b/N_{CH\cdots HC}$ converge to constant values. In fact, there is an excellent correlation between ΔE_b and N_{CH} as well as between ΔE_b and $N_{CH\cdots CH}$, leading to a group increment value of 6.0 kJ mol^{-1} per C−H bond and 2.3 kJ mol^{-1} for CH···HC interaction. Thus, a prediction that follows is that the binding energy of the [146]graphane dimer will be around 439 kJ mol^{-1}, virtually as strong as the bond energy in the H_2 molecule! This adhesion makes the graphane sheets a matrix for many applications.

Table 4. Number of CH Bonds of Each Monomer [n]graphane Involved in the Bonding Area (N_{CH}), Number of Total CH···HC Bonds Formed in Each Dimer ($N_{CH\cdots HC}$), Binding Energy per N_{CH}, and Binding Energy per $N_{CH\cdots HC}$ (kJ mol^{-1})

n	N_{CH}	$N_{CH\cdots HC}$	ΔE_b	$\Delta E_b/N_{CH}$	$\Delta E_b/N_{CH\cdots HC}$
6	3	6	−11.4	−3.8	−1.9
10	5	11	−21.8	−4.4	−2.0
13	7(6)	15	−30.6	−4.4	−2.1
16	8	19	−39.5	−4.9	−2.1
24	12	30	−64.7	−5.4	−2.2
27	14 (13)	34	−70.7	−5.1	−2.1
33	18 (15)	42	−92.4	−5.1	−2.2
37	19 (18)	48	−101.0	−5.3	−2.1
46	25 (21)	60	−134.6	−5.4	−2.3
54	27	72	−164.6	−6.1	−2.3
57	28 (29)	73	−161.4	−5.8	−2.2
61	33 (28)	81	−184.7	−5.6	−2.3
73	37 (36)	99	−216.5	−5.9	−2.2

CONCLUSIONS

The interaction between graphane layers is dominated by London dispersion, with a significant contribution of charge-transfer binding.[33] The latter further shortens the distance between the layers and shifts the electron density to the boundary area between them, forming a glue-like electron density enhancement. It is pleasing to know that at least 15% of the bonding between these saturated hydrocarbons, namely the charge transfer, can be understood intuitively.

On the other hand, the greater part, London dispersion, remains less physically lucid and is embedded in a vast number of electronically excited Slater determinants in wave function theory or in an empirical add-on (DFT-D3 correction) in density functional theory. Valence bond (VB) theory, with the inclusion of dynamic correlation,[75] describes the latter effect as mutual polarization,[33] which is a stabilizing force between the induced dipoles, given by the rising contributions of the $C^+H^-\cdots H^+C^-$ and $C^-H^+\cdots H^-C^+$ forms to the total VB wave function. The global dispersion interaction we find here may act to dress these structures by dynamic correlation and thereby

DOI: 10.1021/acs.jctc.5b00075
J. Chem. Theory Comput. XXXX, XXX, XXX−XXX

bring about the main binding force of the layers. This aspect, which is less obvious in the BLW analysis of the DFT energy, merits a separate future treatment.

Finally, an important finding in this work is that the additive scaling of the total binding energy scales with the number of C−H bonds in the graphane sheets. This enables the prediction of the binding energy for graphane dimers of any size. But even more importantly, this forms the basis for the generation and refinement of force fields, which can be useful in combined quantum mechanical and molecular mechanical (QM/MM) and molecular dynamics (MD) calculations of larger systems, without and with dopants.

■ ASSOCIATED CONTENT

Supporting Information

Detailed structural and energetic information and correlations between the number of carbon atoms of the graphane monomer and the energy components. This material is available free of charge via the Internet at http://pubs.acs.org.

■ AUTHOR INFORMATION

Corresponding Authors

*E-mail: ymo@wmich.edu.
*E-mail: prs@org.chemie.uni-giessen.de.
*E-mail: jemmis@ipc.iisc.ernet.in.
*E-mail: sason@yfaat.ch.huji.ac.il.

Author Contributions

The manuscript was written through contributions of all authors. All authors have given approval to the final version of the manuscript.

Notes

The authors declare no competing financial interest.

■ ACKNOWLEDGMENTS

The work in HU is supported by the Israel Science Foundation (ISF Grant 1183/13) and a Minerva project grant. Y.M. acknowledges the support by the U.S. National Science Foundation under Grants CHE-1055310 and CNS-1126438. C.W. acknowledges the support by the Fund for Distinguished Young Scientists of Shandong Province (NO.BS2014CL033). J.P.W. thanks the Fonds der Chemischen Industrie for a scholarship.

■ ABBREVIATIONS

VB, valence bond; BLW, block localized wave function; EDA, energy decomposition analyses; DFT, density functional theory

■ REFERENCES

(1) Sluiter, M. H. F.; Kawazoe, Y. Cluster Expansion Method for Adsorption: Application to Hydrogen Chemisorption on Graphene. *Phys. Rev. B* **2003**, *68*, 085410.

(2) Sofo, J. O.; Chaudhari, A. S.; Barber, G. D. Graphane: A Two-Dimensional Hydrocarbon. *Phys. Rev. B* **2007**, *75*, 153401.

(3) Elias, D. C.; Nair, R. R.; Mohiuddin, T. M. G.; Morozov, S. V.; Blake, P.; Halsall, M. P.; Ferrari, A. C.; Boukhvalov, D. W.; Katsnelson, M. I.; Geim, A. K.; Novoselov, K. S. Control of Graphene's Properties by Reversible Hydrogenation: Evidence for Graphane. *Science* **2009**, *323*, 610−613.

(4) Zhou, C.; Chen, S.; Lou, J.; Wang, J.; Yang, Q.; Liu, C.; Huang, D.; Zhu, T. Graphene's Cousin: The Present and Future of Graphane. *Nanoscale Res. Lett.* **2014**, *9*, 26.

(5) Lu, N.; Li, Z.; Yang, J. Electronic Structure Engineering via On-Plane Chemical Functionalization: A Comparison Study on Two-Dimensional Polysilane and Graphane. *J. Phys. Chem. C* **2009**, *113*, 16741−16746.

(6) Pumera, M.; Wong, C. H. A. Graphane and Hydrogenated Graphene. *Chem. Soc. Rev.* **2013**, *42*, 5987−5995.

(7) Poh, H. L.; Sofer, Z.; Pumera, M. Graphane Electrochemistry: Electron Transfer at Hydrogenated Graphenes. *Electrochem. Commun.* **2012**, *25*, 58−61.

(8) Savchenko, A. Transforming Graphene. *Science* **2009**, *323*, 589−590.

(9) Gharekhanlou, B.; Tousaki, S. B.; Khorasani, S. Bipolar Transistor Based on Graphane. *J. Phys. Conf. Ser.* **2010**, *248*, 012061.

(10) Tan, S. M.; Sofer, Z.; Pumera, M. Biomarkers Detection on Hydrogenated Graphene Surfaces: Towards Applications of Graphane in Biosensing. *Electroanalysis* **2013**, *25*, 703−705.

(11) Hussain, T.; Pathak, B.; Ramzan, M.; Maark, T. A.; Ahuja, R. Calcium Doped Graphane As a Hydrogen Storage Material. *Appl. Phys. Lett.* **2012**, *100*, 183902.

(12) Nechaev, Y. S. On the Solid Hydrogen Carrier Intercalation in Graphane-Like Regions in Carbon-Based Nanostructures. *Int. J. Hydrogen Energy* **2011**, *36*, 9023−9031.

(13) Wang, L. F.; Ma, T. B.; Hu, Y. Z.; Wang, H.; Shao, T. M. Ab Initio Study of the Friction Mechanism of Fluorographene and Graphane. *J. Phys. Chem. C* **2013**, *117*, 12520−12525.

(14) Pashangpour, M.; Bagheri, Z.; Ghaffari, V. A Comparison of Electronic Transport Properties of Graphene with Hexagonal Boron Nitride Substrate and Graphane, a First Principle Study. *Eur. Phys. J. B* **2013**, *86*, 269.

(15) Peng, Q.; Liang, C.; Ji, W.; De, S. A Theoretical Analysis of the Effect of the Hydrogenation of Graphene to Graphane on Its Mechanical Properties. *Phys. Chem. Chem. Phys.* **2013**, *15*, 2003−2011.

(16) Wen, X. D.; Yang, T.; Hoffmann, R.; Ashcroft, N. W.; Martin, R. L.; Rudin, S. P.; Zhu, J. X. Graphane Nanotubes. *ACS Nano* **2012**, *6*, 7142−7150.

(17) Costamagna, S.; Neek-Amal, M.; Los, J. H.; Peeters, F. M. Thermal Rippling Behavior of Graphane. *Phys. Rev. B* **2012**, *86*, 041408.

(18) Li, Y. F.; Li, F. Y.; Chen, Z. F. Graphane/Fluorographene Bilayer: Considerable C-H center dot center dot center dot F-C Hydrogen Bonding and Effective Band Structure Engineering. *J. Am. Chem. Soc.* **2012**, *134*, 11269−11275.

(19) Zhang, Y.; Wu, X. J. L.; Q, X.; Yang, J. L. Linear Band-Gap Modulation of Graphane Nanoribbons under Uniaxial Elastic Strain: A Density Functional Theory Study. *J. Phys. Chem. C* **2012**, *116*, 9356−9359.

(20) Popova, N. A.; Sheka, E. F. Mechanochemical Reaction in Graphane under Uniaxial Tension. *J. Phys. Chem. C* **2011**, *115*, 23745−23754.

(21) Da, H. X.; Feng, Y. P.; Liang, G. C. Transition-Metal-Atom-Embedded Graphane and Its Spintronic Device Applications. *J. Phys. Chem. C* **2011**, *115*, 22701−22706.

(22) Flores, M. Z. S.; Autreto, P. A. S.; Legoas, S. B.; Galvao, D. S. Graphene to Graphane: A Theoretical Study. *Nanotechnology* **2009**, *20*, 465704.

(23) Wen, X.-D.; Hand, L.; Labet, V.; Yang, T.; Hoffmann, R.; Ashcroft, N. W.; Oganovd, A. R.; Lyakhov, A. O. Graphane sheets and crystals under pressure. *Proc. Natl. Acad. Sci. U.S.A.* **2011**, *108*, 6833−6837.

(24) Fokin, A. A.; Gerbig, D.; Schreiner, P. R. σ/σ- And π/π-Interactions Are Equally Important: Multilayered Graphanes. *J. Am. Chem. Soc.* **2011**, *133*, 20036−20039.

(25) Dahiyat, B. I.; Mayo, S. L. De Novo Protein Design: Fully Automated Sequence Selection. *Science* **1997**, *278*, 82−87.

(26) Kuhlman, B.; Dantas, G.; Ireton, G. C.; Varani, G.; Stoddard, B. L.; Baker, D. Design of A Novel Globular Protein Fold with Atomic-Level Accuracy. *Science* **2003**, *302*, 1364−1368.

(27) Donald, B. R. *Algorithms in Structural Molecular Biology*; MIT Press: Cambridge, MA, 2011.

(28) Granatier, J.; Pitoňák, M.; Hobza, P. Accuracy of Several Wave Function and Density Functional Theory Methods for Description of

DOI: 10.1021/acs.jctc.5b00075
J. Chem. Theory Comput. XXXX, XXX, XXX−XXX

Noncovalent Interaction of Saturated and Unsaturated Hydrocarbon Dimers. *J. Chem. Theory Comput.* **2012**, *8*, 2282−2292.
(29) Schreiner, P. R.; Chernish, L. V.; Gunchenko, P. A.; Tikhonchuk, E. Y.; Hausmann, H.; Serafin, M.; Schlecht, S.; Dahl, J. E. P.; Carlson, R. M. K.; Fokin, A. A. Overcoming Lability of Extremely Long Alkane Carbon-Carbon Bonds Through Dispersion Forces. *Nature* **2011**, *477*, 308−310.
(30) Fokin, A. A.; Chernish, L. V.; Gunchenko, P. A.; Tikhonchuk, E. Y.; Hausmann, H.; Serafin, M.; Dahl, J. E. P.; Carlson, R. M. K.; Schreiner, P. R. Stable Alkanes Containing Very Long Carbon−Carbon Bonds. *J. Am. Chem. Soc.* **2012**, *134*, 13641−13650.
(31) Janowski, T.; Pulay, P. A Benchmark Comparison of σ/σ- And π/π Dispersion: the Dimers of Naphthalene and Decalin, and Coronene and Perhydrocoronene. *J. Am. Chem. Soc.* **2012**, *134*, 17520−17525.
(32) Grimme, S. Do Special Noncovalent $\pi-\pi$ Stacking Interactions Really Exist? *Angew. Chem., Int. Ed.* **2008**, *47*, 3430−3434.
(33) Danovich, D.; Shaik, S.; Neese, F.; Echeverría, J.; Aullón, G.; Alvarez, S. Understanding the Nature of the CH···HC Interactions in Alkanes. *J. Chem. Theory Comput.* **2013**, *9*, 1977−1991.
(34) Alonso, M.; Woller, T.; Martín-Martínez, F. J.; Contreras-García, J.; Geerlings, P.; De Proft, F. Understanding the Fundamental Role of π/π, σ/σ, and σ/π Dispersion Interactions in Shaping Carbon-Based Materials. *Chem.—Eur. J.* **2014**, *20*, 4931−4941.
(35) Mo, Y.; Bao, P.; Gao, J. Energy Decomposition Analysis Based on a Block-Localized Wavefunction and Multistate Density Functional Theory. *Phys. Chem. Chem. Phys.* **2011**, *13*, 6760−6775.
(36) Mo, Y.; Gao, J.; Peyerimhoff, S. D. Energy Decomposition Analysis of Intermolecular Interactions Using a Block-Localized Wave Function Approach. *J. Chem. Phys.* **2000**, *112*, 5530−5538.
(37) Mo, Y.; Peyerimhoff, S. D. Theoretical Analysis of Electronic Delocalization. *J. Chem. Phys.* **1998**, *109*, 1687−1697.
(38) Kitaura, K.; Morokuma, K. A New Energy Decomposition Scheme for Molecular Interactions within the Hartree-Fock Approximation. *Int. J. Quantum Chem.* **1976**, *10*, 325−340.
(39) Morokuma, K. Why Do Molecules Interact? The Origin of Electron Donor-Acceptor Complexes, Hydrogen Bonding and Proton Affinity. *Acc. Chem. Res.* **1977**, *10*, 294−300.
(40) Bagus, P. S.; Hermann, K.; Bauschlicher, C. W., Jr. A New Analysis of Charge Transfer and Polarization for Ligand-Metal Bonding: Model Studies of Carbonylaluminum (Al4CO) and Ammineraluminum (Al4NH3). *J. Chem. Phys.* **1984**, *80*, 4378−4386.
(41) Chen, W.; Gordon, M. S. Energy Decomposition Analyses for Many-Body Interaction and Applications to Water Complexes. *J. Phys. Chem.* **1996**, *100*, 14316−14328.
(42) Glendening, E. D.; Streitwieser, A. Natural Energy Decomposition Analysis - An Energy Partitioning Procedure for Molecular-Interactions with Application to Weak Hydrogen-Bonding, Strong Ionic, and Moderate Donor-Acceptor Interactions. *J. Chem. Phys.* **1994**, *100*, 2900−2909.
(43) Hayes, I. C.; Stone, A. J. An Intermolecular Perturbation Theory for the Region of Moderate Overlap. *Mol. Phys.* **1984**, *53*, 83−105.
(44) Jeziorski, B.; Moszynski, R.; Szalewicz, K. Perturbation Theory Approach to Intermolecular Potential Energy Surfaces of van der Waals Complexes. *Chem. Rev.* **1994**, *94*, 1887−1930.
(45) Rajchel, L.; Żuchowski, P. S.; Szczęśniak, M. M.; Chałasiński, G. Density functional theory approach to noncovalent interactions via monomer polarizations and Pauli blockade. *Phys. Rev. Lett.* **2010**, *104*, 163001.
(46) Reinhardt, P.; Piquemal, J.-P.; Savin, A. Fragment-Localized Kohn−Sham Orbitals via A Singles Configuration-Interaction Procedure and Application to Local Properties and Intermolecular Energy Decomposition analysis. *J. Chem. Theory Comput.* **2008**, *4*, 2020−2029.
(47) Stevens, W. J.; Fink, W. H. Frozen Fragment Reduced Variational Space Analysis of Hydrogen Bonding Interactions. Application to the Water Dimer. *Chem. Phys. Lett.* **1987**, *139*, 15−22.
(48) Stone, A. J. *The Theory of Intermolecular Forces*; Oxford University Press: United Kingdom, 2013.
(49) Su, P.; Li, H. Energy Decomposition Analysis of Covalent Bonds and Intermolecular Interactions. *J. Chem. Phys.* **2009**, *131*, 014101.
(50) van der Vaart, A.; Merz, K. M., Jr. Divide and Conquer Interaction Energy Decomposition. *J. Phys. Chem. A* **1999**, *103*, 3321−3329.
(51) Wu, Q.; Ayers, P. W.; Zhang, Y. K. Density-Based Energy Decomposition Analysis for Intermolecular Interactions with Variationally Determined Intermediate State Energies. *J. Chem. Phys.* **2009**, *131*, 164112.
(52) Ziegler, T.; Rauk, A. On the Calculation of Bonding Energies by the Hartree Fock Slater Method. *Theor. Chem. Acc.* **1977**, *46*, 1−10.
(53) Steinmann, S. N.; Corminboeuf, C.; Wu, W.; Mo, Y. Dispersion-Corrected Energy Decomposition Analysis for Intermolecular Interactions Based on the BLW and dDXDM Methods. *J. Phys. Chem. A* **2011**, *115*, 5467−5477.
(54) Grimme, S.; Antony, J.; Ehrlich, S.; Krieg, H. A Consistent and Accurate Ab Initio Parametrization of Density Functional Dispersion Correction (DFT-D) for the 94 Eements H-Pu. *J. Chem. Phys.* **2010**, *132*, 154104.
(55) Goerigk, L.; Grimme, S. A Thorough Benchmark of Density Functional Methods for General Main Group Thermochemistry, Kinetics, and Noncovalent Interactions. *Phys. Chem. Chem. Phys.* **2011**, *13*, 6670−6688.
(56) Grimme, S. Semiempirical GGA-Type Density Functional Constructed with a Long-Range Dispersion Correction. *J. Comput. Chem.* **2006**, *27*, 1787−1799.
(57) Schmidt, M. W.; Baldridge, K. K.; Boatz, J. A.; Elbert, S. T.; Gordon, M. S.; Jensen, J. J.; Koseki, S.; Matsunaga, N.; Nguyen, K. A.; Su, S.; Windus, T. L.; Dupuis, M.; Montgomery, J. A. General Atomic and Molecular Electronic Structure System. *J. Comput. Chem.* **1993**, *14*, 1347−1363.
(58) Kim, K. S.; Karthikeyan, S.; Singh, N. J. How Different Are Aromatic π Interactions from Aliphatic π Interactions and Non-π Stacking Interactions? *J. Chem. Theory Comput.* **2011**, *7*, 3471−3477.
(59) Boys, S. F.; Bernardi, F. The Calculation of Small Molecular Interaction by the Differences of Separate Total Energies: Some Procedures with Reduced Errors. *Mol. Phys.* **1970**, *19*, 553−566.
(60) Jiemchooroj, A.; Sernelius, B. E.; Norman, P. C6 Dipole-Dipole Dispersion Coefficients for the n-Alkanes: Test of An Additivity Procedure. *Phys. Rev. A* **2004**, *69*, 044701.
(61) Alabugin, I. V.; Gilmore, K. M.; Peterson, P. W. Hyperconjugation. *WIREs Comput. Mol. Sci.* **2011**, *1*, 109−141.
(62) Bickelhaupt, F. M.; Baerends, E. J. The case for steric repulsion causing the staggered conformation of ethane. *Angew. Chem., Int. Ed.* **2003**, *42*, 4183−4188.
(63) Mo, Y.; Wu, W.; Song, L.; Lin, M.; Zhang, Q.; Gao, J. The magnitude of hyperconjugation in ethane: A perspective from ab initio valence bond theory. *Angew. Chem., Int. Ed.* **2004**, *43*, 1986−1990.
(64) Pophristic, V.; Goodman, L. Hyperconjugation not steric repulsion leads to the staggered structure of ethane. *Nature* **2001**, *411*, 565−568.
(65) Schreiner, P. R. Teaching the Right Reasons: Lessons from the Mistaken Origin of the Rotational Barrier in Ethane. *Angew. Chem., Int. Ed.* **2002**, *41*, 3579−3581.
(66) Weinhold, F. Rebuttal to the Bickelhaupt−Baerends Case for Steric Repulsion Causing the Staggered Conformation of Ethane. *Angew. Chem., Int. Ed.* **2003**, *42*, 4188−4194.
(67) Mulliken, R. S.; Parr, R. G. Linear-combination-of-atomic-orbital-molecular-orbital computation of resonance energies of benzene and butadiene, with general analysis of theoretical versus thermochemical resonance energies. *J. Chem. Phys.* **1951**, *19*, 1271−1278.
(68) Mo, Y.; Gao, J. Theoretical analysis of the rotational barrier of ethane. *Acc. Chem. Res.* **2007**, *40*, 113−119.
(69) Reed, A. E.; Curtiss, L. A.; Weinhold, F. Intermolecular interactions from a natural bond orbital, donor-acceptor viewpoint. *Chem. Rev.* **1988**, *88*, 899−926.

DOI: 10.1021/acs.jctc.5b00075
J. Chem. Theory Comput. XXXX, XXX, XXX−XXX

(70) Weinhold, F.; Landis, C. *Valency and Bonding*; Cambridge University Press: Cambridge, UK, 2005.
(71) Joseph, J.; Jemmis, E. D. Red-, Blue-, or No-Shift in Hydrogen Bonds: A Unified Explanation. *J. Am. Chem. Soc.* **2007**, *129*, 4620−4632.
(72) Mo, Y.; Wang, C.; Guan, L.; Braïda, B.; Hiberty, P. C.; Wu, W. On the Nature of Blue shifting Hydrogen Bonds. *Chem.—Eur. J.* **2014**, *20*, 8444−8452.
(73) Rohrer, J.; Hyldegard, P. Stacking and band structure of van der Waals bonded graphane multilayers. *Phys. Rev. B* **2011**, *83*, 165423.
(74) Engler, E. M.; Andose, J. D.; Schleyer, P. v. R. Critical evaluation of molecular mechanics. *J. Am. Chem. Soc.* **1973**, *95*, 8005−8025.
(75) Hiberty, P. C.; Humbel, S.; Archirel, P. Nature of the differential electron correlation in three-electron bond dissociation. Efficiency of a simple two-configuration valence bond method with breathing orbitals. *J. Phys. Chem.* **1994**, *98*, 11697−11704.

DOI: 10.1021/acs.jctc.5b00075
J. Chem. Theory Comput. XXXX, XXX, XXX−XXX